solids

MDPI

Article

Early Strength and Microscopic Mechanisms of Alkali-Metal Hydroxide-Activated Tungsten Tailings

Shanmei Li [1,*], Lei Wang [2], Zhikui Liu [1] and Kai Shou [1]

[1] School of Civil Engineering, Guilin University of Technology, No. 12 Jiangan Rd., Guilin 541004, China; liuzhikui@163.com (Z.L.); kburning@outlook.com (K.S.)
[2] Sinohydro Engineering Bureau 8 Co., Ltd., No. 8 Changqing Rd., Changsha 410000, China; w1309550606@outlook.com
* Correspondence: lishanmei@glut.edu.cn

Abstract: The excellent mechanical properties of alkaline-activated tailings are essential for their increased use in building materials. While numerous studies have been conducted on activated tailings, the strength of alkaline-activated tungsten slag has not been extensively explored due to the low reactivity of silicon and aluminum in these tailings. This research delves into the early unconfined compressive strength of tungsten tailings activated by two alkali solutions (NaOH and KOH) at three different alkali concentrations (mass ratio of alkali to tungsten tailings), cured at 80 °C over periods of one day, three days, and seven days. The study finds significant improvements in the stability of tungsten tailings when forming (C, N)-A-S-H or (C, K)-A-S-H gels with both alkalis. Scanning Electron Microscope (SEM) results show that the morphology of the (C, N)-A-S-H gels transitions from membranous to flocculated and then to a three-dimensional network as the NaOH content and curing time increase. Conversely, the (C, K)-A-S-H gels primarily exhibit thin-film morphology with some three-dimensional network structures. The presence of flocculation and three-dimensional mesh in the gels fosters the formation of a robust skeletal structure, enhancing the strength of the samples. Furthermore, specimens treated with NaOH solution exhibit a higher gel content compared to those treated with KOH solution. These factors contribute to the superior efficacy of sodium hydroxide in enhancing the strength of tungsten tailings compared to potassium hydroxide. X-ray Diffraction (XRD) and Fourier Transform Infrared Spectroscopy (FTIR) results identify the formation of new phases such as pirssonite, buetschliite, potassium bicarbonate, and potassium carbonate. The first new phase results from the carbonization of excess NaOH solution, while the latter phases arise from the carbonization of excess KOH solution. These carbonization processes negatively impact the strength of the materials.

Keywords: alkali activation; tungsten slag; unconfined compressive strength; (C; N)-A-S-H; (C; K)-A-S-H

Citation: Li, S.; Wang, L.; Liu, Z.; Shou, K. Early Strength and Microscopic Mechanisms of Alkali-Metal Hydroxide-Activated Tungsten Tailings. *Solids* **2024**, *5*, 544–560. https://doi.org/10.3390/solids5040037

Academic Editor: Adrián Durán Benito

Received: 4 September 2024
Revised: 27 October 2024
Accepted: 30 October 2024
Published: 12 November 2024

1. Introduction

In 1940, Purdon discovered that the hydration reaction of cement could be significantly accelerated by adding a small amount of sodium hydroxide to the cement slurry. The sodium hydroxide acted as a catalyst, swiftly dissolving the aluminum silicate components and subsequently precipitating calcium silicate and calcium aluminate [1]. Building on this foundational work, J. Davidovits [2] has since made substantial advancements in characterizing the mechanical properties of polymers and has confirmed their applications across various fields. The alkali activation process involves the disruption of Si-O and Al-O bonds in silicon and aluminum-based materials within a strong alkaline environment. This leads to the formation of $[SiO_4]^{4-}$ and $[AlO_4]^{5-}$ monomers. These monomers initially form weaker polymers, such as Si-O-Si or Si-O-Al, which through further polymerization, develop into a more robust alumino-silicate framework.

Mine slag, a solid waste product of the mining industry, is primarily stored in tailing depots or backfilled into mines. This practice occupies significant land and contributes to environmental pollution. Tailings primarily comprise silicon, aluminum, and calcium elements that are key to alkali activation reactions [3]. Consequently, tailings hold the potential for producing alkali-activated materials (AAMs). Extensive research indicates that AAMs possess superior mechanical properties, as well as enhanced resistance to acids, alkalis, and chemicals, surpassing those of Portland cement [4–6]. Additionally, the production of AAMs addresses the high energy consumption and pollution issues associated with Portland cement production, garnering widespread attention for the application of tailings in civil engineering. Numerous studies [7–11] have demonstrated that the mechanical properties of AAMs depend on the type of alkali activator, alkali content, and the composition of the raw materials, among other factors. The primary hydration products in AAMs are layered and catenulate hydrated calcium aluminates (C-A-S-H) gels and hydrated calcium silicate (C-S-H) gels [12,13]. Provis [14] identified that within alkali-activated metakaolin-based materials, the "inner layer" gels are (C, N)-A-S-H, while the "outer layer" gels are C-A-S-H, with both types coexisting in samples—for instance, (C, N)-A-S-H and C-S-H observed in the same specimen [15]. Depending on the silicon-to-aluminum ratio in the activation system, three types of (C, N)-A-S-H gels—PS, PSS, and PSDS—form, each influencing the AAMs' strength differently [16,17]. Clearly, the laws governing and the mechanisms influencing AAMs' strength are complex.

Over the past few decades, numerous researchers have utilized highly active slag [16,18] and fly ash [19,20] as precursors to study the strength of alkali-activated materials. These studies have significantly contributed to the advancement of highly active tailings within the realm of alkali activation. However, the potential of low-activity slags in this field appears to have been overlooked. The question of whether alkali can enhance the strength of low-activity slags remains open for discussion. Predominantly composed of low-reactivity quartz and calcite, tungsten tailings have rarely been the focus of research in alkali-activated materials. This paper aims to explore the early strength and micromechanics of tungsten tailings activated by sodium hydroxide or potassium hydroxide, considering variables such as alkali type, curing time, and alkali content.

2. Materials and Experimental Methods

2.1. Raw Materials

The primary materials utilized in this study are tungsten tailings, sodium hydroxide (NaOH), and potassium hydroxide (KOH). The tungsten tailings, serving as the precursor, are sourced from Guilin in southern China. Sodium hydroxide and potassium hydroxide, used as activators, are produced by China National Pharmaceutical Group Chemical Reagent Co., Ltd. In Nanjing, Jiangsu. The tungsten tailings appear as a gray-white powder with a specific gravity of 2.76. These tailings are characterized by their fine and uniform particles, with more than 84% of the particles distributed between 0.075 mm and 0.2 mm, as detailed in Figure 1. Based on the particle size distribution curve, the tungsten tailings can be classified as fine sand. X-ray diffraction (XRD) was conducted using an X-ray diffractometer (model: ESCALAB 250Xi). The analysis results are presented in Figure 2, revealing that quartz and calcite are the predominant minerals, collectively constituting 74% of the tailings. Additional minor components include kaolin, chlorite, calcareous garnet, pyroxene, and micro-plagioclase. Fluorescence spectrometry was employed to identify the main oxide constituents in the tailings, which include SiO_2, CaO, Fe_2O_3, and Al_2O_3, together accounting for over 88% of the content, alongside trace amounts of MgO, K_2O, SO_3, P_2O_5, etc., as illustrated in Table 1. Microscopic examination (Figure 3) shows that the tungsten tailings primarily exhibit a sheet-like, loose, and disordered structure.

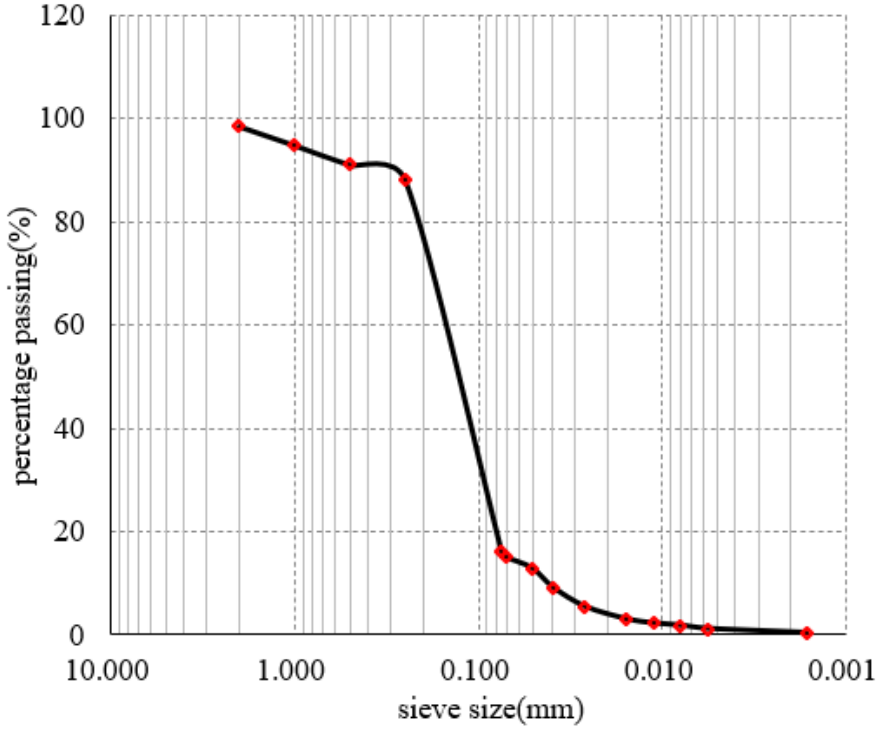

Figure 1. Particle size distribution curve of tungsten tailings.

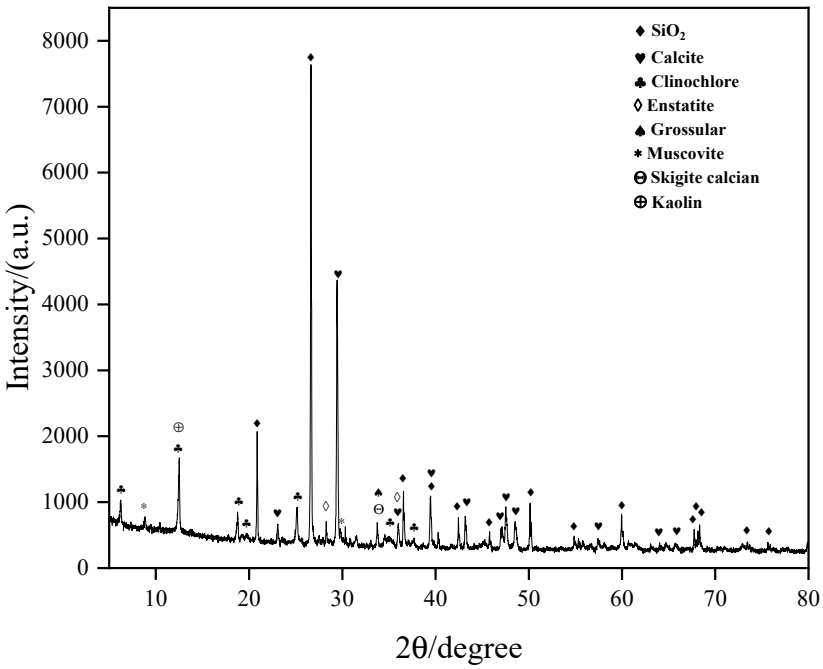

Figure 2. XRD diffractogram of tungsten tailings.

Table 1. Metal oxide composition of tungsten tailings.

Oxide	Content/%
SiO_2	40.05
CaO	29.30
Fe_2O_3	12.42
Al_2O_3	6.90

Table 1. *Cont.*

Oxide	Content/%
MgO	4.33
K_2O	2.12
SO_3	1.67
P_2O_5	0.70
MnO	0.68
TiO_2	0.41
WO_3	0.30
BaO	0.29
PbO	0.24
SnO_2	0.16
Cs_2O	0.08

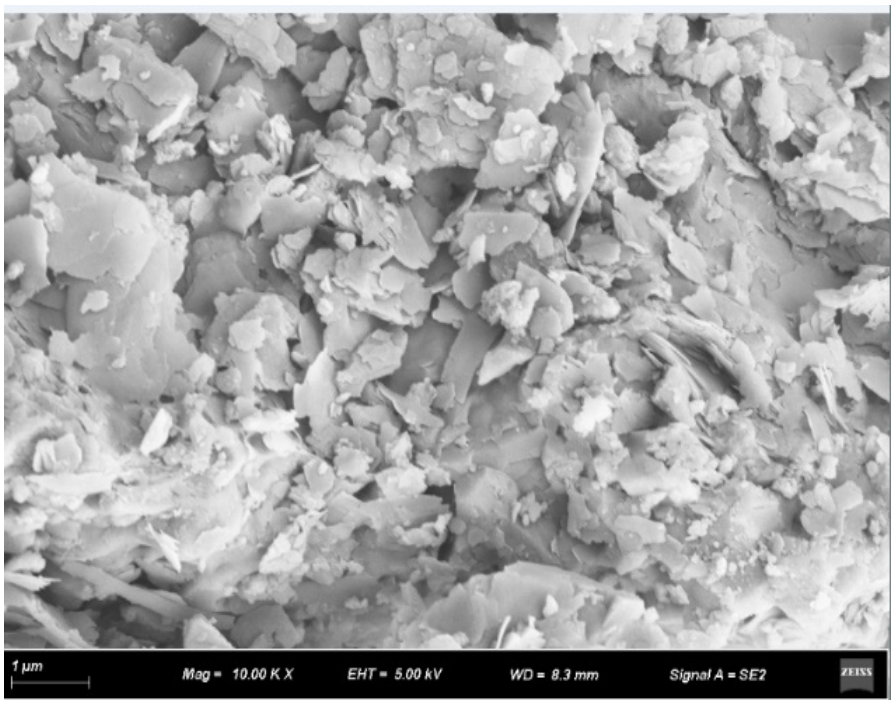

Figure 3. SEM image of tungsten tailing microstructure.

2.2. Sample Preparation and Testing

Each sample comprises 652 g of tungsten tailings, which are crushed and screened through a 10 mesh (2 mm diameter) after being dried in a thermotank at 105 °C for 24 h. Multiple preliminary experiments were conducted to determine the optimal moisture content for sample preparation, based on the workability of the mixture and the quality of the molding. The water mass content for the samples activated by sodium hydroxide and potassium hydroxide solutions is 19% and 16%, respectively. In other words, the moisture content of the sodium hydroxide-excited sample is 19%, whereas the moisture content of the potassium hydroxide-excited sample is 16%. The alkali mass content for all samples treated with NaOH or KOH is set at 5%, 8%, and 11%. To prevent evaporation, the samples were wrapped in plastic wrap and cured in the thermotank at 80 °C for durations of 1 day, 3 days, and 7 days. Detailed information on the sample parameters is provided in Table 2.

Table 2. Sample parameters.

Alkali Type	Alkali Mass Content /%	Water Mass Content /%	Curing Time /d	Tailings Mass /g	Curing Temperature /°C
NaOH	5 8 11	19	1 3 7	652	80
KOH	5 8 11	16	1 3 7	652	80

NaOH and KOH solutions were prepared by dissolving the corresponding alkaline particles in distilled water, as outlined in Table 2. The tailings were then mixed with the cooled (to room temperature, 25 °C) alkali solution and stirred for 10 min. Subsequently, the mixture was placed into a custom 70 mm × 70 mm × 120 mm steel mold, layer by layer. Compression to a height of 70 mm was achieved using the UTM5305 microcomputer-controlled electronic universal testing machine, with an axial compression rate of 0.1 kN/s. After compression, the specimens were demolded using the DTM-150 electric demolding machine. The samples were numbered and wrapped in plastic wrap, then placed in 80 °C thermostats for the designated curing times. According to the experimental protocol, a sheet approximately 2 cm on a side was cut from the demolded specimen's surface and further cured in an 80 °C oven. The microstructure of the sheet was then examined using the GeminiSEM300, operating at a working voltage of 5 kV and a magnification of 10,000 times.

Before testing, all specimens were allowed to cool to room temperature. The unconfined compressive strength of the specimens was measured using the UTM5305 universal testing machine, which applied an axial compression rate of 4 kN/s. The mineral composition of the specimens was analyzed using an X-ray diffraction instrument. X-ray photoelectron spectroscopy was performed with an ESCALAB 250Xi spectrometer, equipped with an aluminum X-ray source and operating under ultra-high vacuum conditions below 10^{-8} Pa. The scanning angle ranged from 5° to 80°, with a scanning speed of 2° per minute. Additionally, functional groups of the specimens were analyzed using a Thermo Nicolet NEXUS 670 Fourier-transform infrared-Raman spectrometer (FTIR). The instrument's spectral range was 4000 cm^{-1} to 400 cm^{-1}, with sample preparation and testing conducted using the KBr method.

3. Experimental Results

3.1. Unconfined Compressive Strength

Figure 4 illustrates the relationship between the unconfined compressive strength of tailings activated by NaOH or KOH, varying by alkali content and curing times. The figure indicates that the strength of samples generally increases with NaOH content, particularly for those with extended curing periods. Specifically, samples activated by NaOH at 5% and 8% content initially show an increase in strength, which then decreases, but strength again increases for those with 11% NaOH content as curing times lengthen. On average, the strength of samples activated with 5%, 8%, and 11% NaOH content increases by factors of 2.3, 2.7, and 4.0, respectively, as the curing period extends from 1 day to 7 days. Conversely, the 1-day and 3-day compressive strengths of samples activated by KOH decrease, while the 7-day strengths initially increase before decreasing as the KOH content rises. The strength of samples activated by KOH, however, consistently increases with curing age, with increases of 3.9, 9.5, and 5.7 times, respectively, when the curing period extends from 1 day to 7 days. The optimal NaOH content is determined to be 11%, yielding a 7-day compressive strength of 30.4 MPa, while the optimal KOH content is 8%, resulting in a 7-day compressive strength of 18.5 MPa.

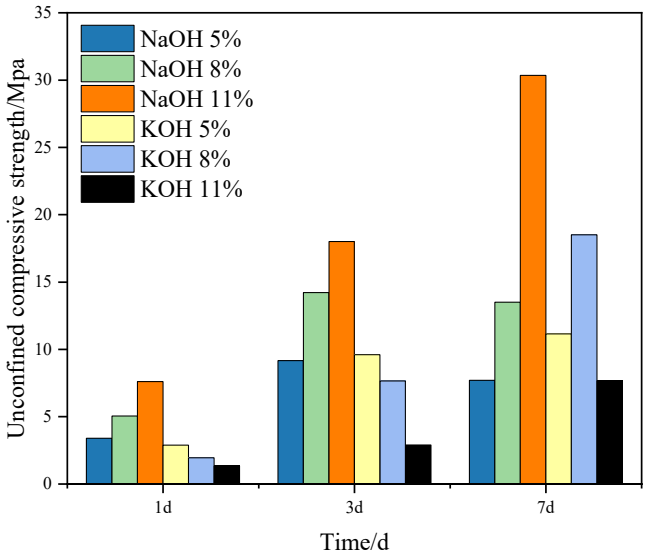

Figure 4. Compressive strength for tungsten tailings activated with NaOH and KOH solution and cured at 80 °C for different times.

3.2. XRD Analysis

Figure 5 presents the X-ray diffraction test patterns of tailings activated by NaOH or KOH. It reveals that the primary original phase components of the tailings, including quartz, calcite, diagonal chlorite, enstatite, calcium-aluminum-garnet, calcium-ferrite, and muscovite, remain intact. However, the peak at 12.5 2θ shows a significant decrease, which can be attributed to the alkali's influence. This reduction is primarily due to the chemical interaction between kaolin and the alkali, as detailed in Formula (1). Additionally, the intensity of the quartz peaks decreases with an increase in alkali content and curing times, a phenomenon explained by Formula (2).

$$Al_2Si_2O_5(OH)_4 + 6OH^- + H_2O \Rightarrow 2Al(OH)_4^- + 2H_2SiO_4^{2-} \quad (1)$$

$$2OH^- + SiO_2 \Rightarrow SiO_3^{2-} + H_2O \quad (2)$$

A new phase, observed between 17 and 18 2θ in the specimens treated with 8% and 11% NaOH content, is highlighted within a purple dotted frame in Figure 5a. This phase is identified as pirssonite ($CaNa_2(CO_3)_2(H_2O)_2$), which forms as a result of the carbonization of excess alkali. This finding aligns with the research conducted by Garcia et al. [21,22]. The pirssonite peaks become progressively sharper and more pronounced as the curing time increases. Additionally, in the samples activated by 5% NaOH, no new characteristic peaks are observed. However, amorphous (N, C)-A-S-H dispersion peaks appear near 12.4, 29, 35, and 42.4 2θ, as indicated by the red, blue, and green lines (number 1, 2, 3) in Figure 5a, reflecting results also noted in previous studies [23].

Figure 5b displays the presence of potassium hydrogen carbonate ($KHCO_3$) and potassium carbonate (K_2CO_3) in samples treated with KOH, corresponding to peaks at 30 and 32.1 2θ, respectively, as indicated by lines 7 and 8 in Figure 5b. Both compounds are products of the carbonization of excess potassium hydroxide. Potassium carbonate deposits on the surface of calcium carbonate form buetschliite ($K_2Ca(CO_3)_2$), which is identified at 31.2 2θ. This formation is pronounced in samples treated with 11% KOH and cured for seven days (see line 9 in Figure 5b)s and is less noticeable in samples treated with 8% KOH and cured for seven days (see line 6 in Figure 5b). This indicates that the formation of buetschliite requires specific concentrations and curing times. Additionally, dispersion peaks of amorphous (K, C)-A-S-H are observed at approximately 12.4, 25.6, and 42.4 2θ.

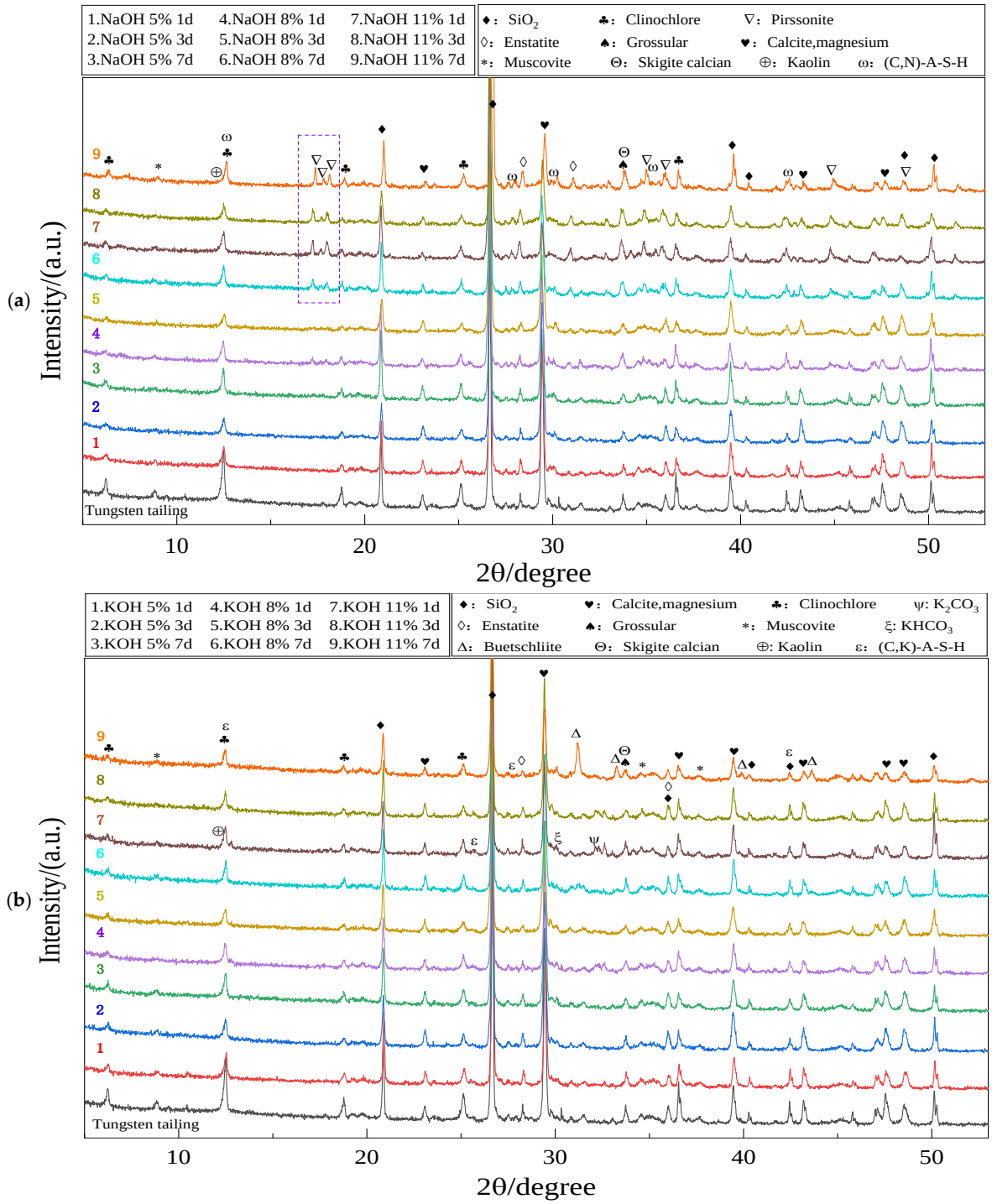

Figure 5. XRD diffractograms of the tungsten tailings activated by (**a**) NaOH; (**b**) KOH and cured at 80 °C for different times.

3.3. SEM-EDS Analysis

Figure 6 illustrates the microstructure of tungsten tailings activated by NaOH and KOH solutions. Due to the similarity in the photos and space constraints, only a selection of representative images are displayed.

Figure 6(a1–a3) depict the microstructural changes in tailings treated with NaOH solutions. As shown, the face-to-face contact sheet structure in tungsten tailings undergoes a noticeable transformation after treatment. The lamellar boundaries become indistinct or disappear altogether due to the formation of new substances, and macrospores significantly

increase. In the N-A-S-H gels, some Na elements are replaced by Ca, forming (C, N)-A-S-H gels [24]. The gel morphologies evolve from thin films to flocculent structures and eventually to three-dimensional networks as the curing time extends from one day to three days and seven days, respectively. The specimens predominantly exhibit a membranous structure at 1 day (see Figure 6(a1)), become flocculent by 3 days (see Figure 6(a2)), and form a three-dimensional network by 7 days (see Figure 6(a3)). The crystallinity of the (C, N)-A-S-H gels improves over time, as evidenced by SEM-EDS analysis. Consequently, spherical particles of pirssonite are observed in samples treated with high-alkali-content solutions (see Figure 6(a2)).

Figure 6(b1–b3) display the microstructure of the tailings activated with KOH solutions, offering a comparison to those treated with NaOH (Figure 6(a1–a3) vs. Figure 6(b1–b3)). The microstructural morphology in specimens treated with KOH solution remains similar to the original tailings but changes over time. The flake boundaries blur due to the formation of membranous gels (Figure 6(b1,b2)), and the formation of three-dimensional network structures causes particles to arrange disorderly (Figure 6(b3)). Bead-like substances stack on the surfaces of flaky minerals, a common feature across all samples. EDS results confirm that the membranous and network substances are (C, K)-A-S-H gels, and the bead-like substance is $K_2Ca(CO_3)_2$, resulting from excess potassium oxide. These findings are consistent with the XRD results shown in Figure 5b, specifically at line 9 ($2\theta = 31°$).

According to the SEM images, the gels exhibit various morphologies, such as membranous, flocculent, and 3D reticular structures. Aluminum and calcium are crucial in determining the nature of the gels that form during alkaline activation [25,26]. Moreover, the influence of alkali metal cations on gel structure also merits consideration. A known challenge in energy spectrum testing is the reduction in spectral test accuracy, particularly in mixtures, where X-rays quickly penetrate surface materials. This makes it difficult to distinguish between Si in gels or quartz, especially given the high quartz content in both raw and alkali-activated minerals. Consequently, this study explores the impact of the relative content of Ca, Al, Na, or K cations in different gels on their morphology. The chemistries are systematically categorized based on the forms of gels as illustrated in Figure 7.

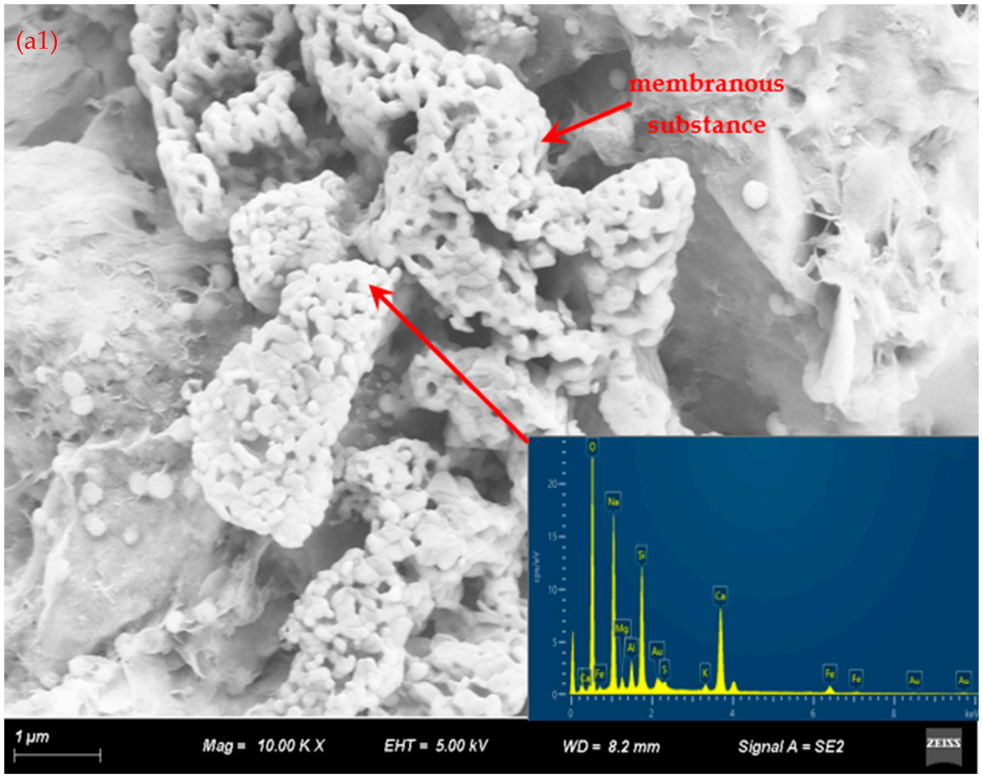

Figure 6. *Cont.*

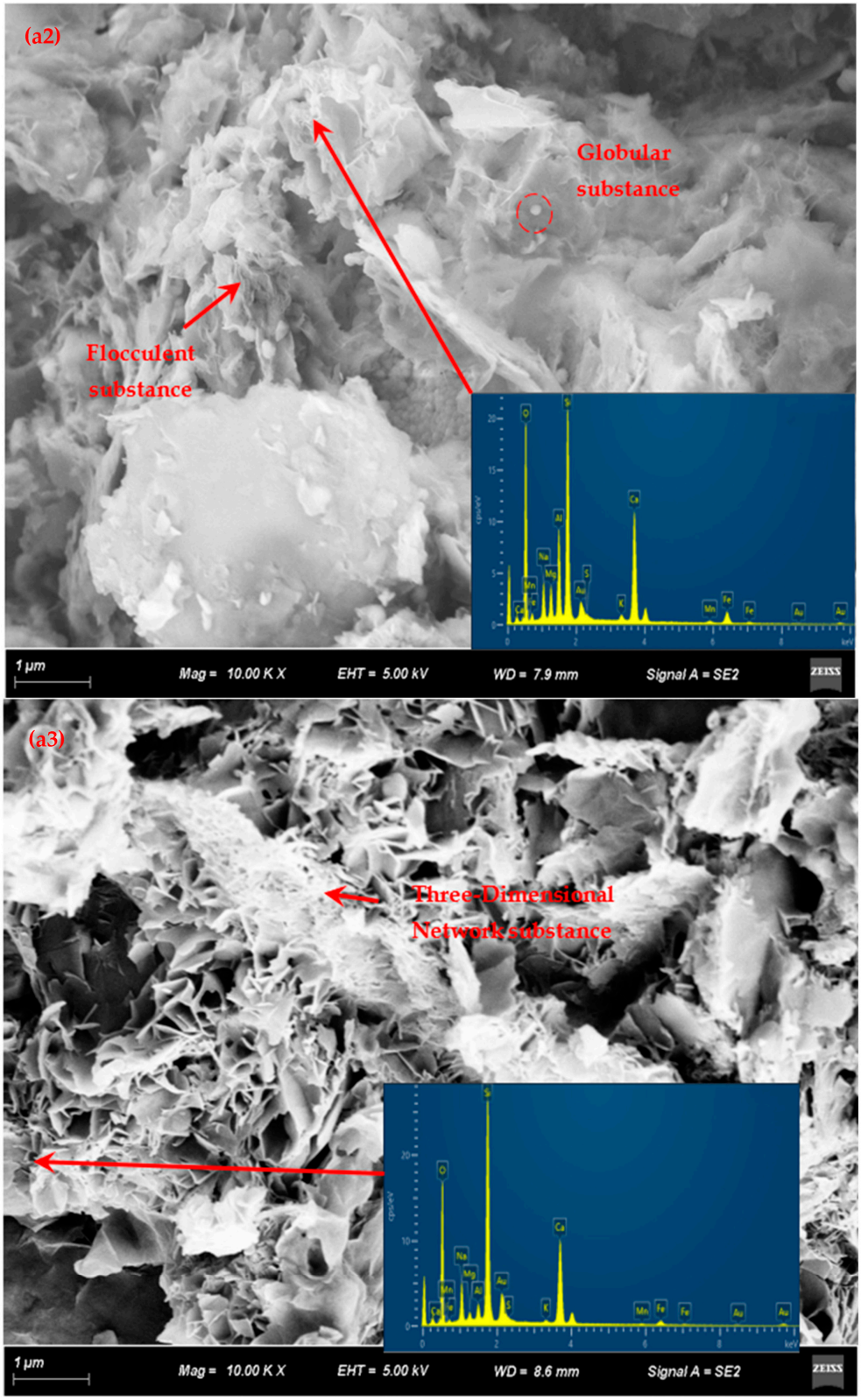

Figure 6. *Cont.*

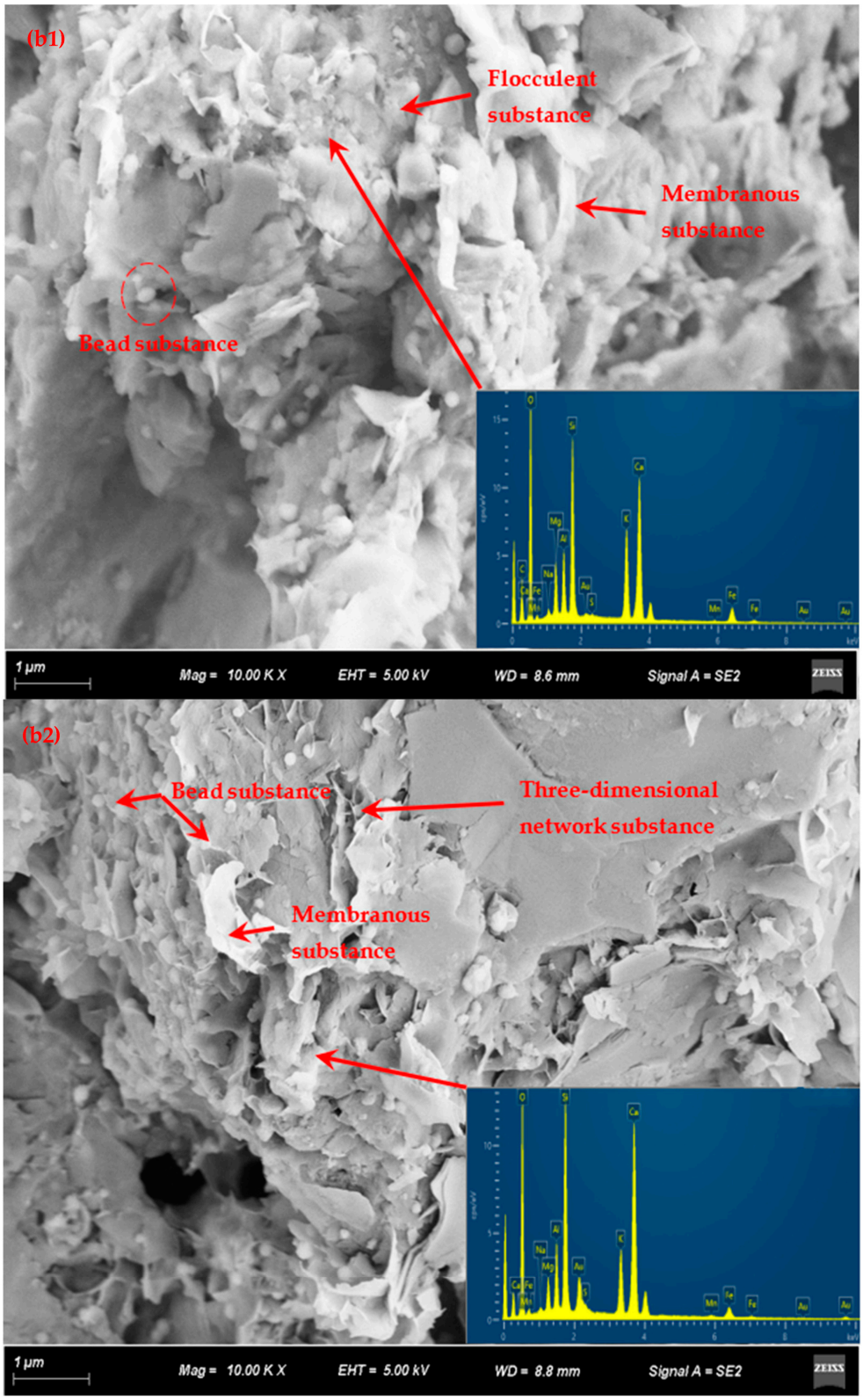

Figure 6. *Cont.*

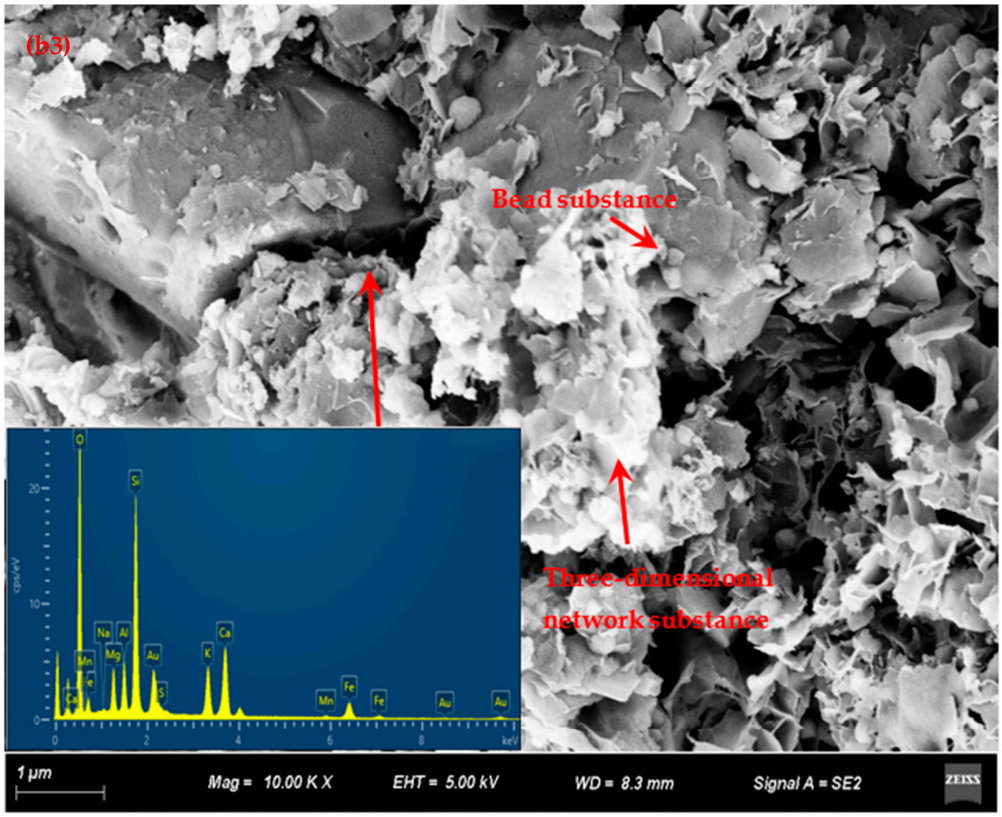

Figure 6. SEM micrographs of tungsten tailings activated by: (**a1**) 5% NaOH, cured for 1 day; (**a2**) 5% NaOH, cured for 3 days; (**a3**) 8% NaOH, cured for 7 days; (**b1**) 8% KOH, cured for 1 day; (**b2**) 8% KOH, cured for 3 days; (**b3**) 8% KOH, cured for 7 days at 80 °C. (Magnification: ×10,000).

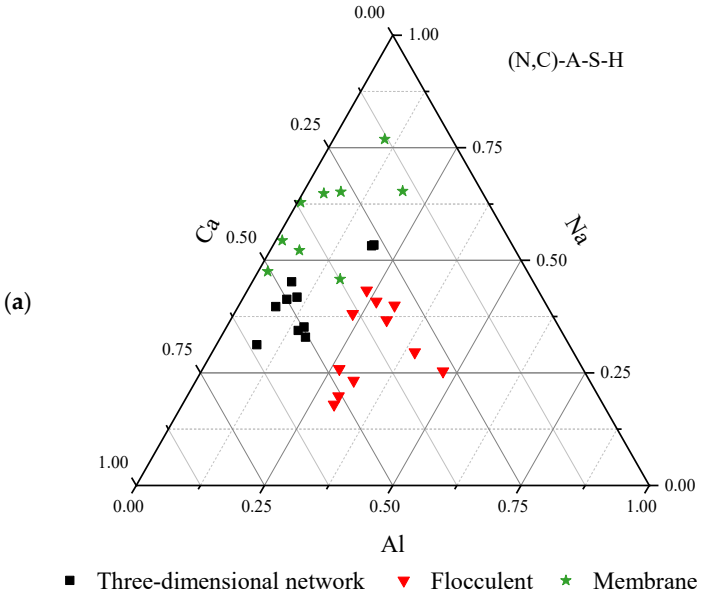

Figure 7. *Cont*.

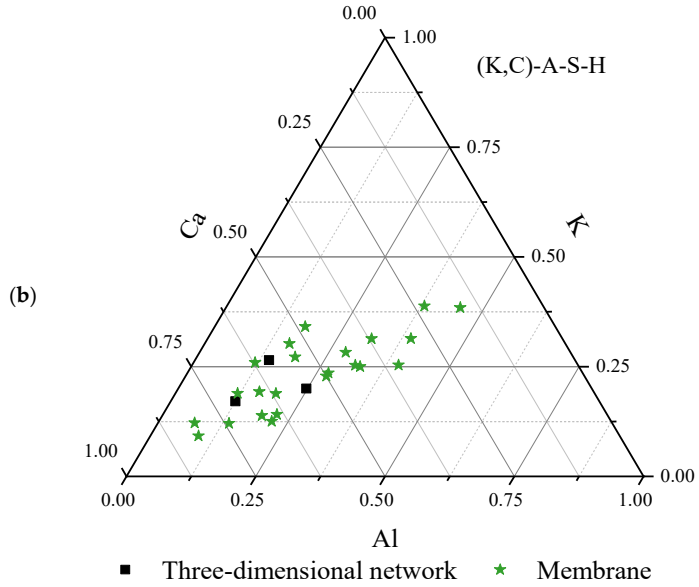

Figure 7. Projection of alkali-activated material (gels) chemistry onto (**a**) the ternary CaO-Al_2O_3-Na_2O system and (**b**) the ternary CaO-Al_2O_3-K_2O system, excluding SiO_2 content: elemental composition of tungsten slag cured for seven days as determined by SEM-EDS analysis.

In Figure 7a, the elements of (N, C)-A-S-H gels formed from specimens activated by NaOH solutions predominantly spread from the middle section towards the left. The morphologies of (N, C)-A-S-H gels demonstrate a clear regularity in the pseudo ternary phase diagram. The membranous gels, three-dimensional reticular gels, and flocculent gels are distributed on the left, middle, and right sections, respectively. For the membranous gels, the relative content of Na is comparatively high, ranging from 0.5 to 0.75, while Al content is lower, ranging from 0 to 0.25, and Ca content is moderate, situated between 0.1 and 0.5. Regarding the three-dimensional reticular gels, the relative Ca content is high, primarily between 0.5 and 0.75, Al content is lower, around 0.25, and Na content is moderate, specifically between 0.25 and 0.5. For the flocculent gels, the relative content of Ca is high, mainly between 0.55 and 0.85, while Al and Na are comparably balanced, primarily ranging from 0.25 to 0.5.

In Figure 7b, the elements of (K, C)-A-S-H gels, generated from specimens activated by KOH solutions, are primarily distributed from the middle to the bottom in a linear fashion. These gels predominantly consist of a thin primary film with fewer reticular structures. Notably, the relative content of Ca in the (K, C)-A-S-H membrane gels is significantly higher than in the (N, C)-A-S-H gels, typically ranging from about 0.5 to 0.9.

3.4. FTIR Analysis

Figure 8 displays the Fourier Transform Infrared (FTIR) spectroscopy results for tailings activated by NaOH or KOH at alkali contents of 5%, 8%, and 11%, after curing for one, three, and seven days, respectively. As illustrated in Figure 8, most peak positions remain consistent, though the widths of the peaks change, and new absorption peaks emerge at certain locations, depending on the type and concentration of the alkali activator used.

The signals between 1420 cm^{-1} and 1490 cm^{-1} arise from the asymmetric stretching vibrations of C-O bonds [27], with the peak at 1420 cm^{-1} being the characteristic absorption peak for $CaCO_3$, indicating a substantial presence of calcite in the tailings. Notably, some spectra (e.g., lines 2, 3, 6, 8, and 9) show shoulder absorption peaks at these wavenumbers due to $Na_2Ca(H_2O)_2[CO_3]_2$, formed by excess NaOH solution, as depicted in Figure 8a. Additionally, new absorption peaks at 1560 cm^{-1} (e.g., lines 1, 2, and 3) and 1480 cm^{-1} (e.g., lines 5 and 6) emerge, corresponding to K_2CO_3 and $KHCO_3$ formed by excess KOH solution, as shown in Figure 8b. These findings are in line with the XRD analyses.

The bending vibration of the T(Si/Al)-O bonds at 463 cm^{-1} is intensified by the alkali [28], although this effect diminishes with increased curing time and alkali concentration, suggesting a reduction in T-O bonds as activated Si/Al participates in the reaction to form polymerization. The main band (T-O-T: Si or Al) is situated at wavenumbers around 650 cm^{-1}, 1000 cm^{-1}, and 1090 cm^{-1}, indicative of the formation of (C, N)-A-S-H or (C, K)-A-S-H gels [29,30].

The O-H bond signals spanning 3200 cm^{-1} to 3600 cm^{-1} [31] show a shift from 3450 cm^{-1} to 3420 cm^{-1} with increased curing time when treated with alkali solutions, as depicted in Figure 8a. This shift indicates a change in the length of the O-H bonds in the structural water of gels with increasing curing age and alkali content. Comparatively, the O-H peak intensity for polymers treated with NaOH is stronger than that for those treated with KOH, as shown by comparing Figure 8a,b, suggesting a greater gel production from NaOH treatment [32].

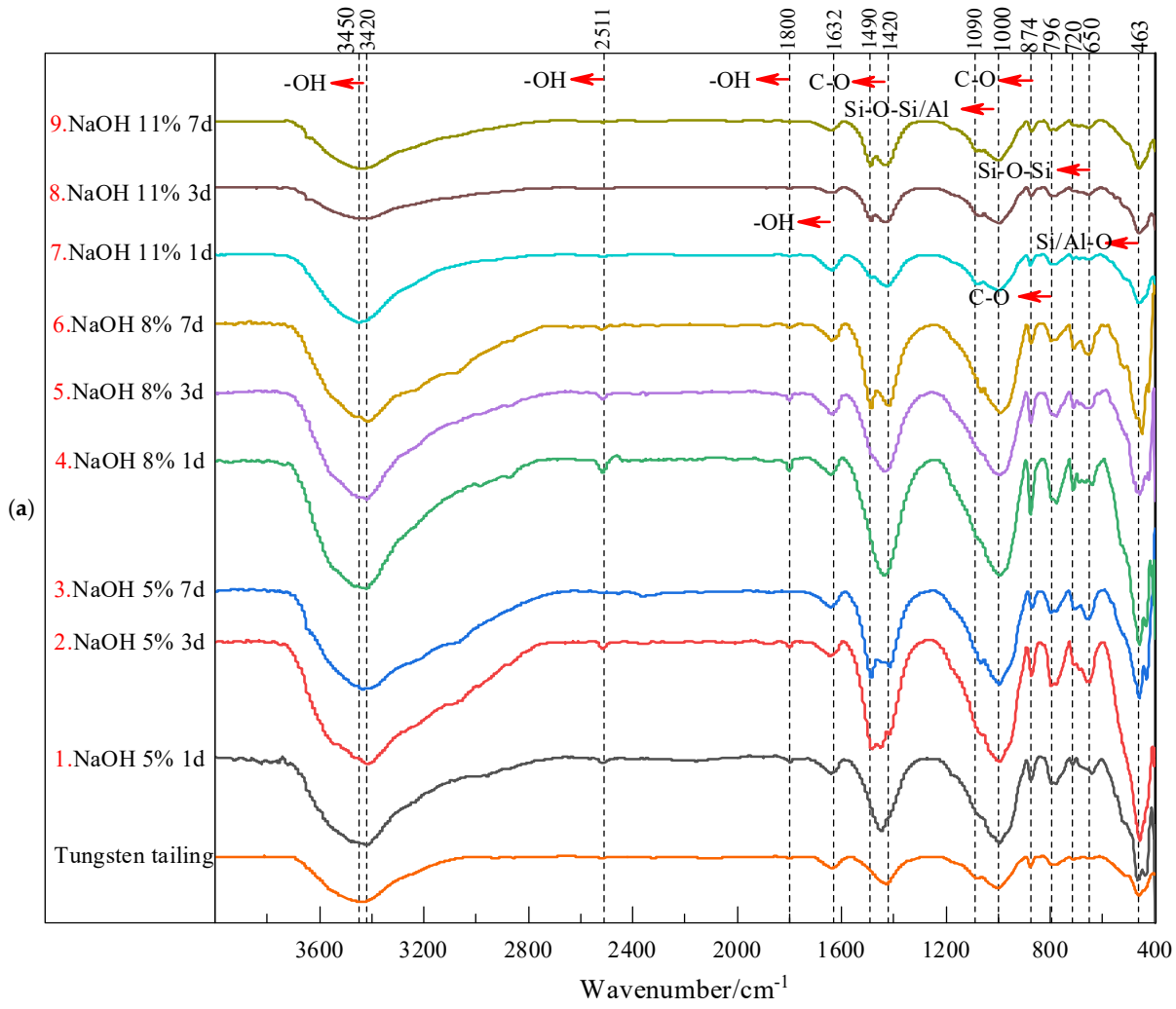

Figure 8. *Cont.*

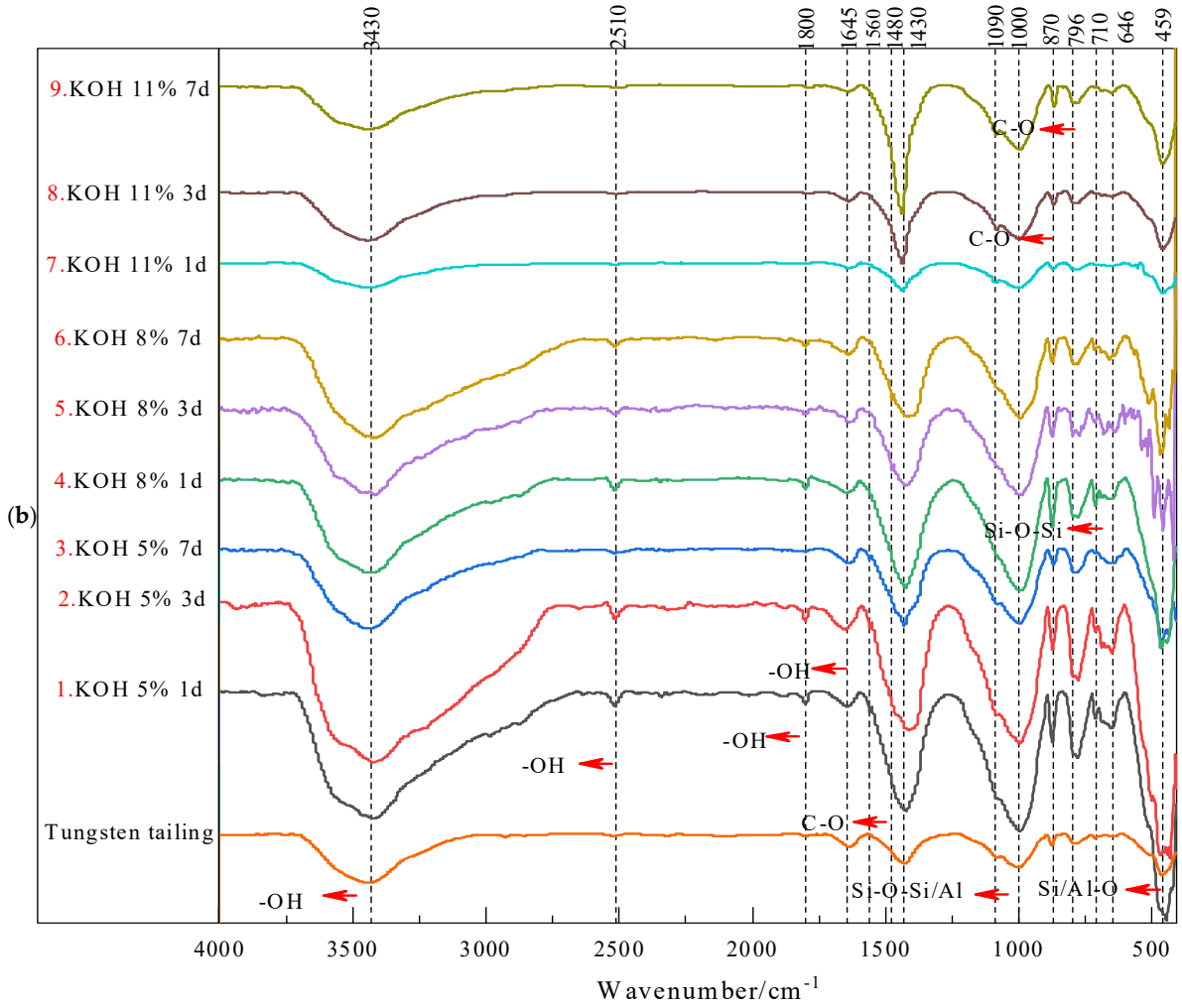

Figure 8. FTIR spectra of tungsten tailings activated by (**a**) NaOH and (**b**) KOH.

The O-H bond signals spanning 3200 cm^{-1} to 3600 cm^{-1} [31] show a shift from 3450 cm^{-1} to 3420 cm^{-1} with increased curing time when treated with alkali solutions, as depicted in Figure 8a. This shift indicates a change in the length of the O-H bonds in the structural water of gels with increasing curing age and alkali content. Comparatively, the O-H peak intensity for polymers treated with NaOH is stronger than that for those treated with KOH, as shown by comparing Figure 8a,b, suggesting a greater gel production from NaOH treatment [32].

4. Discussions

Geopolymers are classified into C-A-S-H and N-A-S-H types based on the calcium content of the alkali-activated system. Similarly, when potassium hydroxide is used as the activator, K-A-S-H gel is formed. In highly alkaline environments, Ca/K-O and T-O-T (tetrahedral Si or Al) bonds are broken down from the minerals. This leads to the depolymerization of Si and Al into monomers which eventually form gels. The specific process of gel formation is outlined as follows.

$$x\mathrm{SiO}_3^{2-} + y\mathrm{AlO}_2^- + n\mathrm{OH}^- + m\mathrm{Na}^+ + z\mathrm{H_2O} \Rightarrow (\text{N-A-S-H}) \quad (3)$$

$$x\mathrm{SiO}_3^{2-} + y\mathrm{AlO}_2^- + n\mathrm{OH}^- + m\mathrm{K}^+ + z\mathrm{H_2O} \Rightarrow (\text{K-A-S-H}) \quad (4)$$

$$x\mathrm{SiO}_3^{2-} + y\mathrm{AlO}_2^- + n\mathrm{OH}^- + m\mathrm{Ca}^{2+} + z\mathrm{H_2O} \Rightarrow (\text{C-A-S-H}) \quad (5)$$

The depolymerization and polycondensation of tetrahedrons in tailings can be accelerated in a high-alkali environment, which enhances the hydration reaction and the rate of gel formation. The formation of gels in samples treated with NaOH increases with the alkali content, contributing positively to the unconfined compressive strength of the material. At the initial stages of curing, rapid excitation within the tailings leads to gel formation in this high-alkali environment. This results in ions dissolved on the surface of the tailings being unable to diffuse outward, as the gels quickly encapsulate the tailing particles, preventing further hydration within the particles. This phenomenon is pivotal to the observed low strength of the sample at early curing stages. As the curing time and NaOH content increase, more gels are generated and the crystallinity of these gels improves, both of which are key factors contributing to the increased strength of materials activated with NaOH over time.

As the curing time and alkali content increase, the number of formed colloids also increases, and theoretically, the crystallinity of these colloids should improve. However, no significant diffraction peaks were observed around 30 degrees (2θ) in the XRD patterns (as shown in Figure 5), and similar peaks were even found in the original tailings. Additionally, different gel morphologies were observed in the scanning electron microscope (SEM) analysis (as shown in Figure 6(a3)); however, no clear evidence of enhanced crystallinity was found. Therefore, this suggests that the (C, N)-A-S-H and (C, K)-A-S-H phases exhibit a high degree of amorphousness.

Similarly, the increase in gel quantity and higher crystallinity are also reasons for the strength enhancement in KOH-activated tungsten tailings over time. However, excessive KOH tends to form buetschliite (as shown in Figure 5b), which is detrimental to the material's strength. Consequently, the strength of KOH-activated tungsten tailings decreases with increasing KOH concentration.

The influence of NaOH and KOH solutions on strength shows significant differences, despite both being strong alkalis. The reasons for these differences can be attributed to three main factors:

1. Dissolving Power: NaOH has a stronger capability than KOH to dissolve SiO_2 and Al_2O_3 [33]. Consequently, specimens treated with NaOH tend to form more gels than those treated with an equivalent concentration of KOH, as evidenced by SEM images (see Figure 7). A higher quantity of gels correlates with increased compressive strength.

2. Crystallization Tendency: The gel materials excited by KOH exhibit a lower tendency to crystallize [34], resulting in a slower rate of strength development after tailing activation. A comparison of Figure 7a,b reveals that a large number of flocculent and 3D reticular crystalline gels appear in samples activated by NaOH and cured for three days, whereas only a small amount of 3D reticular gels are present in those activated by KOH and cured for seven days.

3. Ionic Radius and Permeability: The ionic radius of sodium hydrate is smaller than that of potassium hydrate, leading to greater permeability. As a result, the reaction speed and gel formation in a NaOH environment are more efficient than in a KOH environment. This was verified by research from Duxson [35].

These factors illustrate why NaOH generally enhances the mechanical properties of alkali-activated materials more effectively than KOH.

5. Conclusions

This study investigated the unconfined compressive strength of tungsten tailings activated with NaOH and KOH, considering variables such as alkali type, content, and curing time. The strength mechanisms were analyzed using SEM, XRD, and FTIR techniques, yielding the following conclusions:

1. The unconfined compressive strength of the samples positively correlates with both the curing time and NaOH content but shows a negative correlation with KOH content (except for samples cured for seven days). At the same alkali content and curing age, samples activated with NaOH demonstrate higher strength than those activated with KOH.

2. XRD analyses indicate that the main mineral phases in the raw tailings remain unchanged post-alkali activation, but a high degree of amorphousness gel-phase substances are produced. (C, N)-A-S-H gels form in samples treated with NaOH and increase with rising alkali concentration. The morphology of these gels evolves from thin films to flocculation and then to a three-dimensional network as the curing time progresses. Conversely, (C, K)-A-S-H gels, which form in KOH-treated tailings, are less abundant than (C, N)-A-S-H gels and exhibit poor crystallization, typically appearing as thin films with some three-dimensional networks.

3. With increasing alkali content, carbonation occurs in the specimens. NaOH-activated samples carbonize into pirssonite, whereas KOH-activated samples lead to the formation of buetschliite, $KHCO_3$, and K_2CO_3.

4. NaOH proves more effective than KOH at enhancing the strength of tungsten tailings. Based on the unconfined compressive strength observed, the optimal contents of NaOH and KOH in this study are 11% and 8%, respectively.

The results highlight that the early strength of alkali-activated tungsten tailings is substantial. However, the long-term strength and durability of this material remain unknown. These properties are crucial for the broader adoption of such materials. Therefore, future research should focus on the long-term strength and durability of these materials to further substantiate their viability.

Author Contributions: S.L.: Formulation or evolution of overarching research goals and aims, experimental method, revise the paper, provide funding. L.W.: Principal tester, writing and reviewing the paper. Z.L.: Conception and experimental design. K.S.: Assist the test. All authors have read and agreed to the published version of the manuscript.

Funding: This research was funded by the National Natural Science Foundation of China (52268055) and the Natural Science Foundation of Guangxi Zhuang Autonomous Region (2023GXNSFBA026269).

Data Availability Statement: Data will be made available upon request.

Conflicts of Interest: Author Lei Wang was employed by the company "Sinohydro Engineering Bureau 8 Co.". The remaining authors declare that the research was conducted in the absence of any commercial or financial relationships that could be construed as a potential conflict of interest.

References

1. Purdon, A.O. The action of alkalis on blast-furnace slag. *J. Soc. Chem. Ind.* **1940**, *59*, 191–202.
2. Davidovits, J. 30 years of successes and failures in geopolymer applications. Market trends and potential breakthroughs. In Proceedings of the Geopolymer 2002 Conference, Melbourne, Australia, 28–29 October 2002; pp. 1–16.
3. Pacheco-torgal, J.; Castro-gomes, F.; Jalali, S. Alkali-activated binders: A review Part 1. Historical background, terminology, reaction mechanisms and hydration products. *Constr. Build. Mater.* **2008**, *22*, 1305–1314. [CrossRef]
4. Grzeszczyk, S. The truth about the geopolymers. *Cem. Wapno Beton* **2021**, *26*, 101–108. [CrossRef]
5. Davidovits, J. Environmentally driven geopolymer cement applications. In Proceedings of the Geopolymer 2002 Conference, Melbourne, Australia, 28–29 October 2002; pp. 1–9.
6. Lodeiro, I.G.; Cristelo, N.; Palomo, A.; Fernández-Jiménez, A. Use of industrial by-products as alkaline cement activators. *Constr. Build. Mater.* **2020**, *253*, 119000.1–119000.11. [CrossRef]
7. França, S.; De Moura Solar Silva, M.V.; Borges, P.H.R.; da Silva Bezerra, A.C. A review on some properties of alkali-activated materials. *Innov. Infrastruct. Solut.* **2022**, *7*, 179. [CrossRef]
8. Zivica, V. Effects of type and dosage of alkaline activator and temperature on the properties of alkali-activated slag mixtures. *Constr. Build. Mater.* **2007**, *21*, 1463–1469. [CrossRef]
9. Tanzer, R.; Jin, Y.; Stephan, D. Alkali activated slag binder: Effect of cations from silicate activators. *Mater. Struct.* **2017**, *50*, 91–97. [CrossRef]
10. Aydin, S.; Baradan, B. Effect of activator type and content on properties of alkali-activated slag mortars. *Compos. Part B. Eng.* **2014**, *57B*, 166–172. [CrossRef]
11. Puertas, F.; Amat, T.; Fernandez-Jimenez, A. Mechanical and durable behaviour of alkaline cement mortars reinforced with polypropylene fibres. *Cem. Concr. Res.* **2003**, *33*, 2031–2036. [CrossRef]
12. Samantasinghar, S.; Singh, S. Effects of curing environment on strength and microstructure of alkali-activated fly ash-slag binder. *Constr. Build. Mater.* **2020**, *235*, 117481.1–117481.10. [CrossRef]
13. Provis, J.L.; Bernal, S.A. Geopolymers and Related Alkali-Related Materials. *Annu. Rev. Mater. Res.* **2014**, *44*, 299–327. [CrossRef]

14. Bernal, S.A.; Provis, J.L.; Rose, V.; Gutierrez, R.M.D. High-Resolution X-ray Diffraction and Fluorescence Microscopy Characterization of Alkali-Activated Slag-Metakaolin Binders. *J. Am. Ceram. Soc.* **2013**, *96*, 1951–1957. [CrossRef]
15. He, J.; Bai, W.; Zheng, W.; He, J.; Sang, G. Influence of hydrated lime on mechanical and shrinkage properties of alkali-activated slag cement. *Constr. Build. Mater.* **2021**, *289*, 123201.1–123201.11. [CrossRef]
16. Davidovits, J. Geopolymer technology: The current state of the art. *J. Mater. Sci.* **2007**, *42*, 2917–2933. [CrossRef]
17. Hajimohammadi, A.; Ngo, T.; Kashani, A. Glass waste versus sand as aggregates: The characteristics of the evolving geopolymer binders. *J. Clean. Prod.* **2018**, *193*, 593–603. [CrossRef]
18. Puertas, F.; Gonzalez-Fonteboa, B.; Gonzalez-Taboada, I.; Alonso, M.D.M.; Torres-Carrasco, M.; Rojo, G.; Martínez-Abella, F. Alkali-activated slag concrete: Fresh and hardened behaviour. *Cem. Concr. Compos.* **2018**, *85*, 22–31. [CrossRef]
19. Atabey, I.I.; Karahan, O.; Bilim, C.; Atis, C.D. Very high strength Na_2SiO_3 and NaOH activated fly ash based geopolymer mortar. *Cem. Wapno Beton* **2020**, *25*, 292–305. [CrossRef]
20. Ryu, G.S.; Lee, Y.B.; Koh, K.T.; Chung, Y.S. The mechanical properties of fly ash-based geopolymer concrete with alkaline activators. *Constr. Build. Mater.* **2013**, *47*, 409–418. [CrossRef]
21. Lodeiro, I.G.; Macphee, D.E.; Palomo, A.; Fernandez-Jimenez, A. Effect of alkalis on fresh C–S–H gels. FTIR analysis. *Cem. Concr. Res.* **2009**, *39*, 147–153. [CrossRef]
22. Bernal, S.A.; Provis, J.L.; Walkley, B.; Nicolas, R.S.; Gehman, J.D.; Brice, D.G.; Kilcullen, A.R.; Duxson, P.; van Deventer, J.S.J. Gel nanostructure in alkali-activated binders based on slag and fly ash, and effects of accelerated carbonation. *Cem. Concr. Res.* **2013**, *53*, 127–144. [CrossRef]
23. Kapeluszna, E.; Kotwica, L.; Rozycka, A.; Gołek, Ł. Incorporation of Al in C-A-S-H gels with various Ca/Si and Al/Si ratio: Microstructural and structural characteristics with DTA/TG, XRD, FTIR and TEM analysis. *Constr. Build. Mater.* **2017**, *155*, 643–653. [CrossRef]
24. García-Lodeiro, I.; Fernández-Jiménez, A.; Palomo, A.; Macphee, D.E. Effect of calcium additions on N-A-S-H cementitious gels. *J. Am. Ceram. Soc.* **2010**, *93*, 1934–1940. [CrossRef]
25. Yip, C.K.; Lukey, G.C.; Provis, J.L. Effect of calcium silicate sources on geopolymerisation. *Cem. Concr. Res.* **2008**, *38*, 554–564. [CrossRef]
26. Garcia-Lodeiro, I.; Fernandez-Jimenez, A.; Pena, P. Alkaline activation of synthetic aluminosilicate glass. *Ceram. Int.* **2014**, *40*, 5547–5558. [CrossRef]
27. Puertas, F.; Palacios, M.; Manzano, H.; Dolado, J.S.; Rico, A. Rodríguez. A model for the C-A-S-H gel formed in alkali-activated slag cements. *J. Eur. Ceram. Soc.* **2011**, *31*, 2043–2056. [CrossRef]
28. Ismail, I.; Bernal, S.A.; Provis, J.L.; Nicolas, R.S.; Hamdan, S.; van Deventer, J.S.J. Modification of phase evolution in alkali-activated blast furnace slag by the incorporation of fly ash. *Cem. Concr. Compos.* **2014**, *45*, 125–135. [CrossRef]
29. Fernández-Jiménez, A.; Palomo, A. Mid-infrared spectroscopic studies of alkali-activated fly ash structure. *Microporous Mesoporous Mater.* **2005**, *86*, 207–214. [CrossRef]
30. Garcia-Lodeiro, I.; Palomo, A.; Fernandez-Jimenez, A.; Macphee, D.E. Compatibility studies between N-A-S-H and C-A-S-H gels. Study in the ternary diagram Na_2O-CaO-Al_2O_3-SiO_2-H_2O. *Cem. Concr. Res.* **2011**, *41*, 923–931. [CrossRef]
31. Palomo, A.; Grutzeck, M.W.; Blanco, M.T. Alkali-activated fly ashes a cement for the future. *Cem. Concr. Res.* **1999**, *29*, 1323–1329. [CrossRef]
32. Sha, D.; Pan, B.; Sun, Y. A novel raw material for geopolymers: Coal-based synthetic natural gas slag. *J. Clean. Prod.* **2020**, *262*, 121238.1–121238.14. [CrossRef]
33. Leemann, A.; Saout, G.L.; Winnefeld, F.; Rentsch, D.; Lothenbach, B. Alkali–Silica Reaction: The influence of calcium on silica dissolution and the formation of reaction products. *J. Am. Ceram. Soc.* **2011**, *94*, 1243–1249. [CrossRef]
34. Duxson, P.; Mallicoat, S.W.; Lukey, G.C.; Kriven, W.M.; van Deventer, J.S.J. The effect of alkali and Si/Al ratio on the development of mechanical properties of metakaolin-based geopolymers. *Colloids Surf. A Physicochem. Eng. Asp.* **2007**, *292*, 8–20. [CrossRef]
35. Duxson, P.; Provis, J.L.; Lukey, G.C.; van Deventer, J.S.J. ^{39}K NMR of free potassium in geopolymers. *Ind. Eng. Chem. Res.* **2006**, *45*, 9208–9210. [CrossRef]